

# A numerical simulation study on the impact of smoke aerosols from Russian forest fires on the air pollution over Asia

Qingzhe Zhu, Yuzhi Liu\*, Rui Jia, Shan Hua, Tianbin Shao, Bing Wang

Key Laboratory for Semi-Arid Climate Change of the Ministry of Education, College of Atmospheric Sciences, Lanzhou University, Lanzhou, 730000, China



## ARTICLE INFO

**Keywords:**  
Smoke aerosol  
Transportation  
AOD  
FLEXPART-WRF  
PM10

## ABSTRACT

Serious forest fires were observed over Siberia, particularly in the vast area between Lake Baikal and the Gulf of Ob, during the period of 18–27 July 2016 using Moderate Resolution Imaging Spectroradiometer (MODIS) data. The Cloud-Aerosol Lidar and Infrared Pathfinder Satellite Observations (CALIPSO) satellite simultaneously detected a multitude of smoke aerosols surrounding the same area. Combing a Lagrangian Flexible Particle dispersion model (FLEXPART) executed using the Weather Research and Forecasting (WRF) model output, the transport of smoke aerosols and the quantification of impact of Russian forest fires on the Asia were investigated. From model simulations, two transport paths were determined for the smoke plumes from the Russian forest fires. The first path was directed southwestward from Russia to Central Asia and eventually Xinjiang Province of China, furthermore, the second path was directed southeastward through Mongolia to Northeast China. The FLEXPART-WRF model simulations also revealed that the smoke aerosol concentrations entering the Central Asia, Mongolia and Northern China were approximately  $60\text{--}300 \mu\text{g m}^{-3}$ ,  $40\text{--}250 \mu\text{g m}^{-3}$  and  $5\text{--}140 \mu\text{g m}^{-3}$ , respectively. Meanwhile, the aerosol particles from these forest fires have an impact on the air quality in Asia. With the arrival of smoke aerosols from the Russian forest fires, the near-surface PM10 concentrations over Altay, Hulunbuir and Harbin increased to  $61$ ,  $146$  and  $42 \mu\text{g m}^{-3}$ , respectively. In conclusion, smoke aerosols from Russian forest fires can variably influence the air quality over Central Asia, Mongolia and Northern China.

## 1. Introduction

Suspended solid and liquid particles in the atmosphere known as aerosols (Albrecht, 1989; Haywood and Boucher, 2000) can influence the radiation budget through direct, semi-direct and indirect effects (Han et al., 2013; Huang et al., 2014; Jia et al., 2015; Liu et al., 2013, 2014, 2015) and then impact the regional and global climate systems. Smoke aerosols sourced from biomass burning, especially from forest fires, constitute an important type of aerosol, as they may absorb radiation and therefore partially offset the negative climate forcing of anthropogenic aerosols (Penner et al., 2003). Moreover, smoke aerosols can promote longer-lived clouds with smaller droplets and inhibit precipitation (Koren and Martins, 2004). In addition, smoke aerosols also play a substantial role in both the environment and the atmospheric chemistry (Crutzen and Andreae, 1990; Christopher et al., 1996; Penner et al., 1992). Therefore, smoke aerosols are an important influencing factor on the Earth's climate system.

In addition to influencing the climate at the local scale, smoke aerosols can affect the regional-scale air quality and radiation balance due to vertical ascension above the planetary boundary layer (Kahn

et al., 2008; Martin et al., 2009) and horizontal transport over long distances (Damoah et al., 2004; Forster et al., 2001; Kahn et al., 2007). Solomos et al. (2015) described the local scale features which govern smoke aerosols dispersion. Dirksen et al. (2009) found that a smoke aerosol plume released by a strong forest fire in Australia could circumnavigate the world in 12 days. Miller et al. (2011) showed that smoke aerosols from forest fires in Canada could affect the air quality in the northeastern United States by increasing the PM2.5 concentration by up to  $10\text{--}20 \text{ mg m}^{-3}$  and by increasing the ozone concentration over the East Coast of the United States (Dreessen et al., 2016). The finding of Brioude et al. (2009) underscored biomass burning aerosols have dual effects on cloud radiative forcing. In addition, previous studies have shown that smoke aerosols sourced from China (Noh et al., 2009; Sang et al., 2011; Zhang et al., 2010), South America (Rosário et al., 2013) and the United States (Nopmongcol et al., 2007) can also be transported to their surrounding areas. Therefore, the transport of smoke aerosols must be further investigated with regard to the impacts of such aerosols on the atmospheric environment and climate system.

The Far East and the Siberian region of Russia both possess vast forests. As a consequence, both regions are host to some of the most

\* Corresponding author.

E-mail address: [liuyzh@lzu.edu.cn](mailto:liuyzh@lzu.edu.cn) (Y. Liu).

**Table 1**  
Model configurations and physics options of the WRF model simulation.

WRF microphysics and model configurations	Selection of schemes and configurations
Domain dimensions	340 × 165
Grid size	30 km
Vertical layers	32 layers
Microphysics scheme	WRF 6-class graupel scheme
Long-wave radiation scheme	RRTM scheme
Short-wave radiation scheme	Dudhia scheme
Surface layer scheme	Monin-Obukhov similarity theory
Land-surface scheme	5-layer thermal diffusion
Boundary layer scheme	YSU scheme
Cumulus parameterization scheme	Kain-Fritsch scheme

serious forest fires worldwide. According to statistics compiled by the Russian Federal Forestry Administration, between 17,000 and 33,000 forest fires occur in Russia every year (Conard and Ivanova, 1997; Kozlov et al., 1999; Lee et al., 2005; Müller et al., 2005; Stocks et al., 1998). Some studies reported that smoke aerosols from summer fires in Russia can not only influence the local radiation budget (Chubarova et al., 2012; Gorchakova and Mokhov, 2012; Shukurov et al., 2014; Sitnov et al., 2013) but also affect the air quality over downstream areas; for example, the surface PM10 concentration was correspondingly increased by up to 258  $\mu\text{g m}^{-3}$  in Korea (Lee et al., 2005). In addition, black carbon (BC) from forest fires in Siberia and the Russian Far East can be transported to the Arctic (Vinogradova et al., 2015), and the CO released from such fires could persist at the global scale for up to 17 days (Damoah et al., 2004). Though many studies have been performed concerning the transport of smoke aerosols from Russian forest fires, few studies focused on the impacts of smoke aerosols originating from Russia on neighboring countries, especially China.

In this study, a strong smoke-generating forest fire that occurred in July 2016 in Siberia is identified using Moderate Resolution Imaging Spectroradiometer (MODIS) and Cloud-Aerosol Lidar and Infrared Pathfinder Satellite Observations (CALIPSO) data. Based on the simulation of the Weather Research and Forecasting (WRF) model, the

meteorological conditions during the forest fire event are analyzed. Simultaneously, the WRF model and the Lagrangian Flexible Particle dispersion model (FLEXPART) are employed to simulate the transport of smoke aerosols. Aerosol Robotic Network (AERONET) datasets are also analyzed to confirm the transport of smoke aerosols from Russian forest fires. Finally, air quality measurements and Copernicus Atmosphere Monitoring Service (CAMS) datasets are analyzed to investigate the effects of the smoke aerosols from the July 2016 fires event on the air quality over Northern China.

## 2. Datasets

### 2.1. CALIPSO profiles

The CALIPSO satellite, which was launched on 28 April 2006 by NASA, carries three primary detectors: the Cloud-Aerosol Lidar with Orthogonal Polarization (CALIOP), an Infrared Imaging Radiometer (IIR), and a Wide Field Camera (WFC). The CALIOP sensor is a two-wavelength, polarization-sensitive backscatter lidar that exhibits a strong sensitivity in the detection of aerosols and clouds and can therefore acquire their vertical information. In this study, data consisting of the total and perpendicular attenuated backscatter coefficients at 532 nm from the CALIPSO Level 1B product and data comprising aerosol particle properties from the CALIPSO lidar Vertical Feature Mask (VFM) product are used to identify the smoke events.

### 2.2. MODIS products

MODIS is an optical remote sensor on board the Terra and Aqua satellites that provides global observations at wavelengths ranging from the visible band to the mid-infrared band. The study area, which includes the Central Asian region, encompasses desert and semi-desert regions; therefore, Deep Blue aerosol optical depth (AOD) retrievals from the MOD04\_L2 and MYD04\_L2 products with a 10-km resolution are used to investigate the distribution of smoke aerosols, both kinds of products are combined to fill the gap each other in spatial. The MOD14 Level 3 Thermal Anomalies/Fire product, which is primarily derived

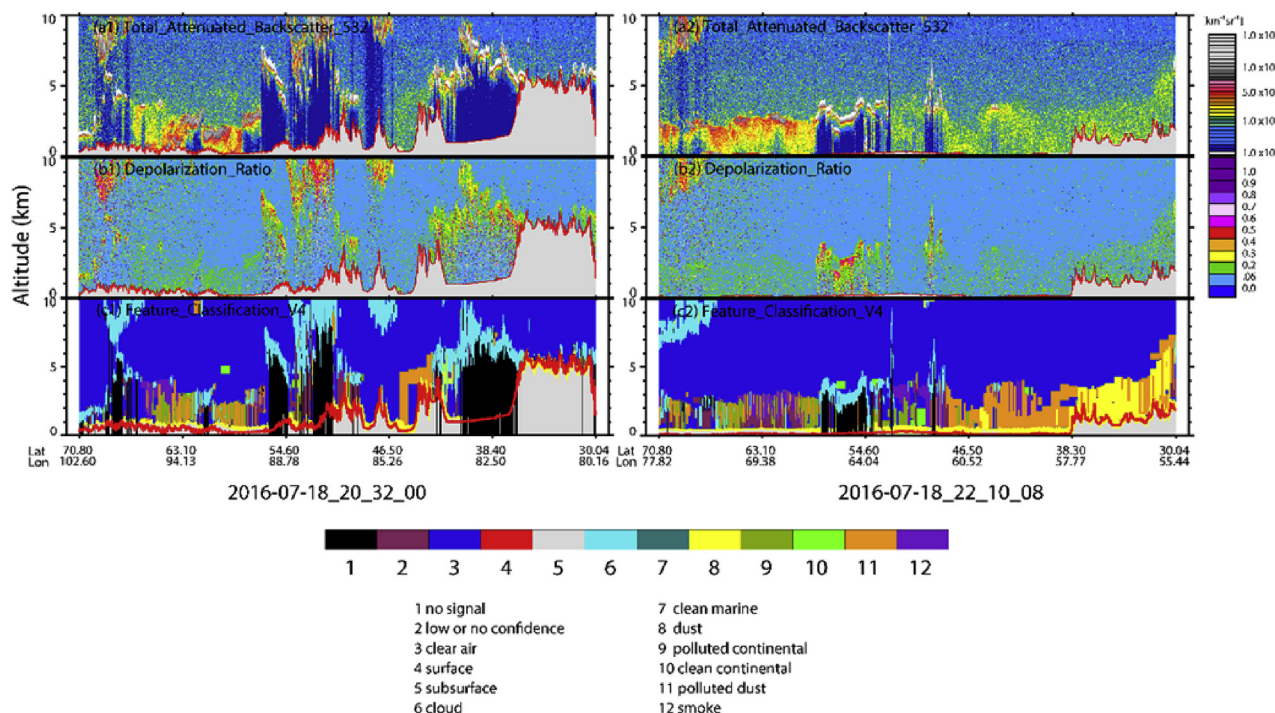


**Fig. 1.** Altitude-orbit cross-sections of the total attenuated backscattering (a1-a2), depolarization ratio (b1-b2) and classified particles (c1-c2) on 18 July 2016 along the trajectory of the CALIPSO satellite over Russia.

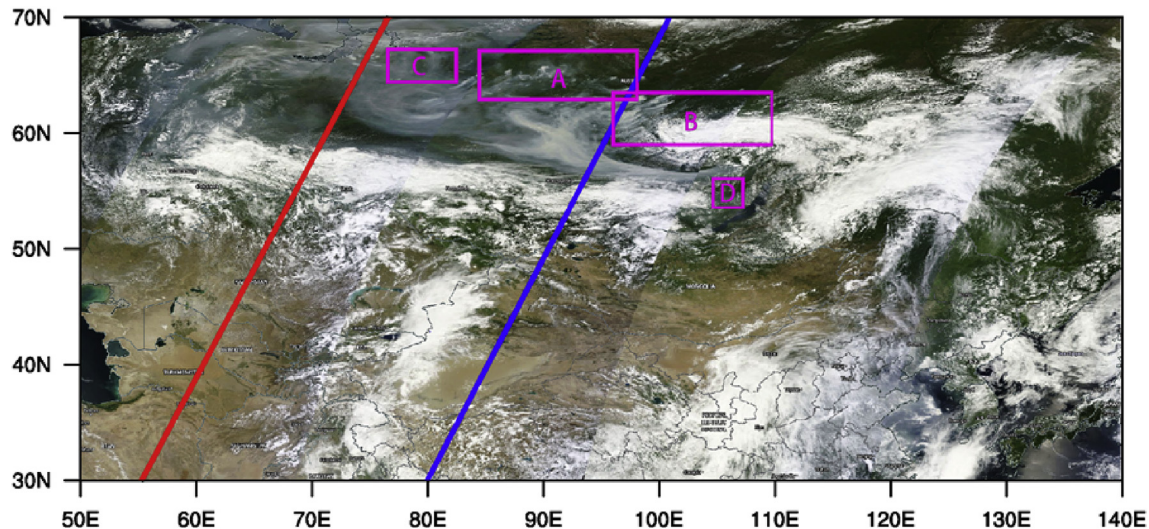


**Fig. 2.** MODIS Terra satellite image over the study area on 18 July 2016. The red and blue lines indicate the trajectory of the CALIPSO satellite on 18 July 2016. The purple boxes indicate the aerosol sources set up in FLEXPART-WRF model. (For interpretation of the references to color in this figure legend, the reader is referred to the Web version of this article.)

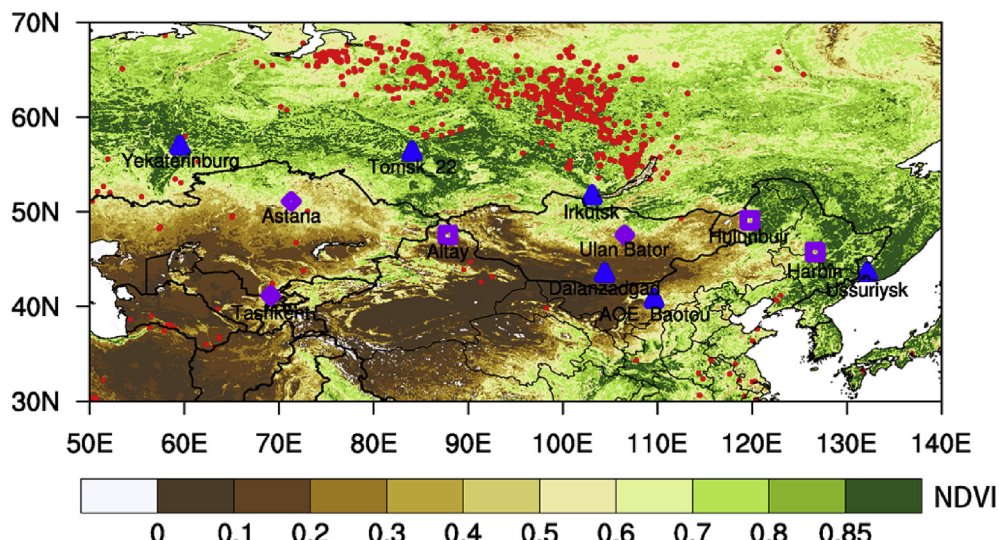


**Fig. 3.** A color plot of the NDVI for July 2016 over the study area with positions of the fires obtained from the MOD14 fire product in 17–28 July 2016. Note that Red dots are the fire hot spots. Blue triangles are AERONET sites. Purple squares are PM10 observation stations. Purple rhombus are cities in Central Asia and Mongolia.

from MODIS 4- and 11- $\mu\text{m}$  radiances, contains the most basic level of MODIS fire data. In this study, the daily MOD14A1 product with a 1-km resolution is used to determine the locations of forest fires. In addition, global MOD13C2 data, which provide a monthly composite of the normalized difference vegetation index (NDVI) with a latitudinal and longitudinal resolution of  $0.05^\circ \times 0.05^\circ$ , are used to display the vegetation coverage of the study area.

### 2.3. Site observations of air particles

AODs derived from AERONET and PM10 data are used in this study. AERONET, which is composed of numerous ground-based remote sensing aerosol networks, can provide the AOD distribution at a global scale. In this study, AERONET Level 1.5 Version 3 data are employed for six sites: Tomsk\_22 ( $56.42^\circ\text{N}$ ,  $84.07^\circ\text{E}$ ), Yekaterinburg ( $57.04^\circ\text{N}$ ,  $59.55^\circ\text{E}$ ), Irkutsk ( $51.80^\circ\text{N}$ ,  $103.09^\circ\text{E}$ ), Dalanzadgad ( $43.58^\circ\text{N}$ ,  $104.42^\circ\text{E}$ ), AOE\_Baotou ( $40.85^\circ\text{N}$ ,  $109.63^\circ\text{E}$ ) and Ussuriysk ( $43.70^\circ\text{N}$ ,  $132.16^\circ\text{E}$ ). Meanwhile, to estimate the contributions from smoke plumes originating from Russia to the air pollution over Northern

China, PM10 data (<https://pan.baidu.com/s/1gd8GUxt#list/path=%2F>) from three China Environmental Monitoring Network stations, namely, Hulunbuir ( $49.12^\circ\text{N}$ ,  $119.73^\circ\text{E}$ ), Harbin ( $45.75^\circ\text{N}$ ,  $126.63^\circ\text{E}$ ) and Altay ( $47.56^\circ\text{N}$ ,  $87.84^\circ\text{E}$ ), are utilized in this study.

### 2.4. ECMWF data

ECMWF ERA5 reanalysis data (Hersbach, 2016) and CAMS data are used to analyze the meteorological conditions and the transport of smoke aerosols. Hourly vertical velocity from the ERA5 dataset are employed. The reanalysis data have a spatial (latitudinal and longitudinal) resolution of  $0.5^\circ \times 0.5^\circ$  and 37 pressure levels in the vertical direction. The CAMS, which is operated by ECMWF, provides reliable information regarding the composition and variations of the atmosphere. The CAMS product includes data concerning solar radiation, particulates that affect the air quality, pollen, and greenhouse gases. In this study, AOD data for different aerosol types with a spatial resolution of  $0.5^\circ \times 0.5^\circ$  and wildfire flux data of BC with a spatial resolution of  $0.1^\circ \times 0.1^\circ$  are used.

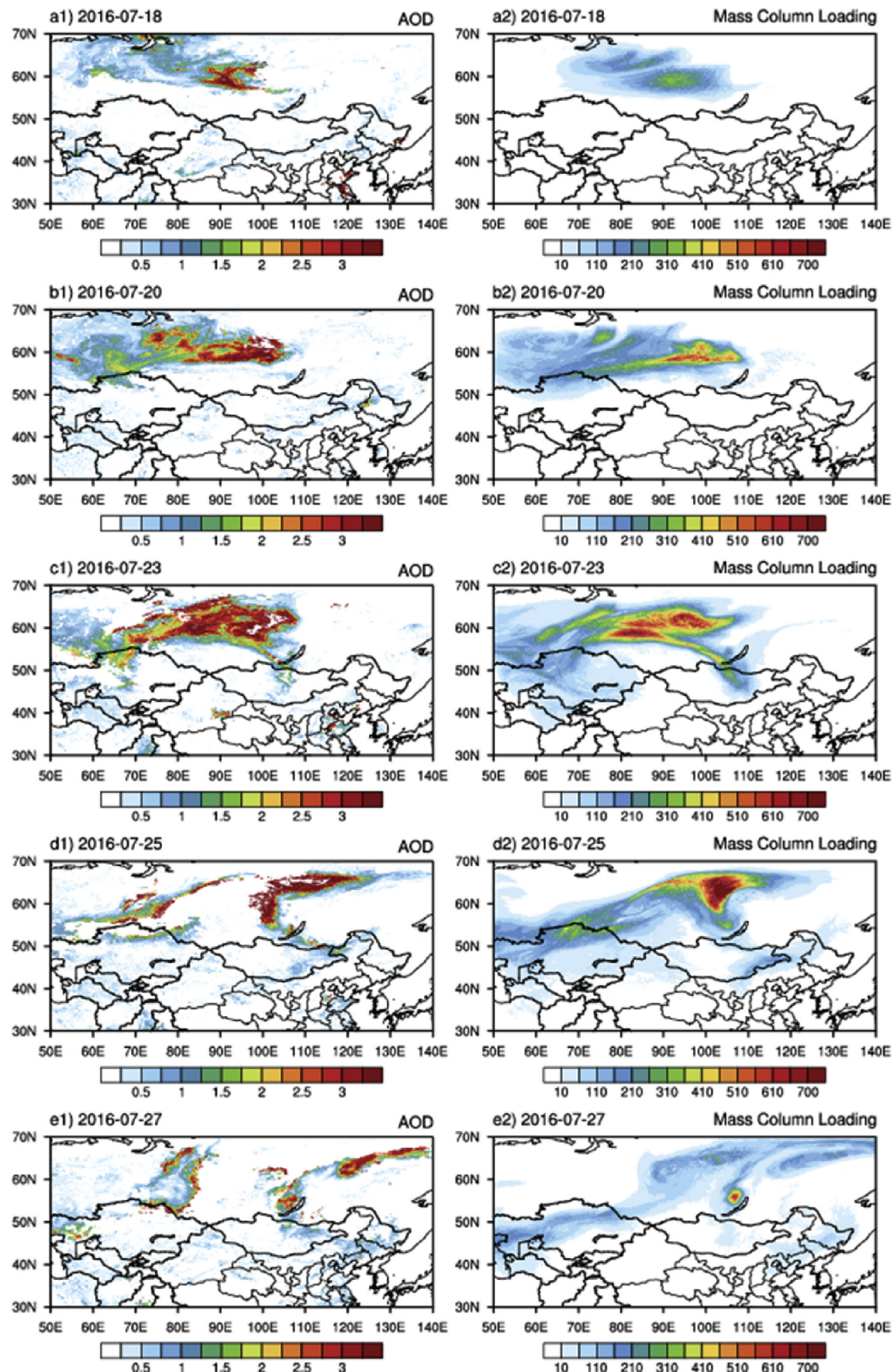


**Fig. 4.** Distributions of the AOD from MODIS (a1-e1) and the aerosol mass column loading values (units:  $\text{mg m}^{-2}$ ) simulated using the FLEXPART-WRF model (a2-e2) on 18 July, 20 July, 23 July, 25 July and 27 July 2016.

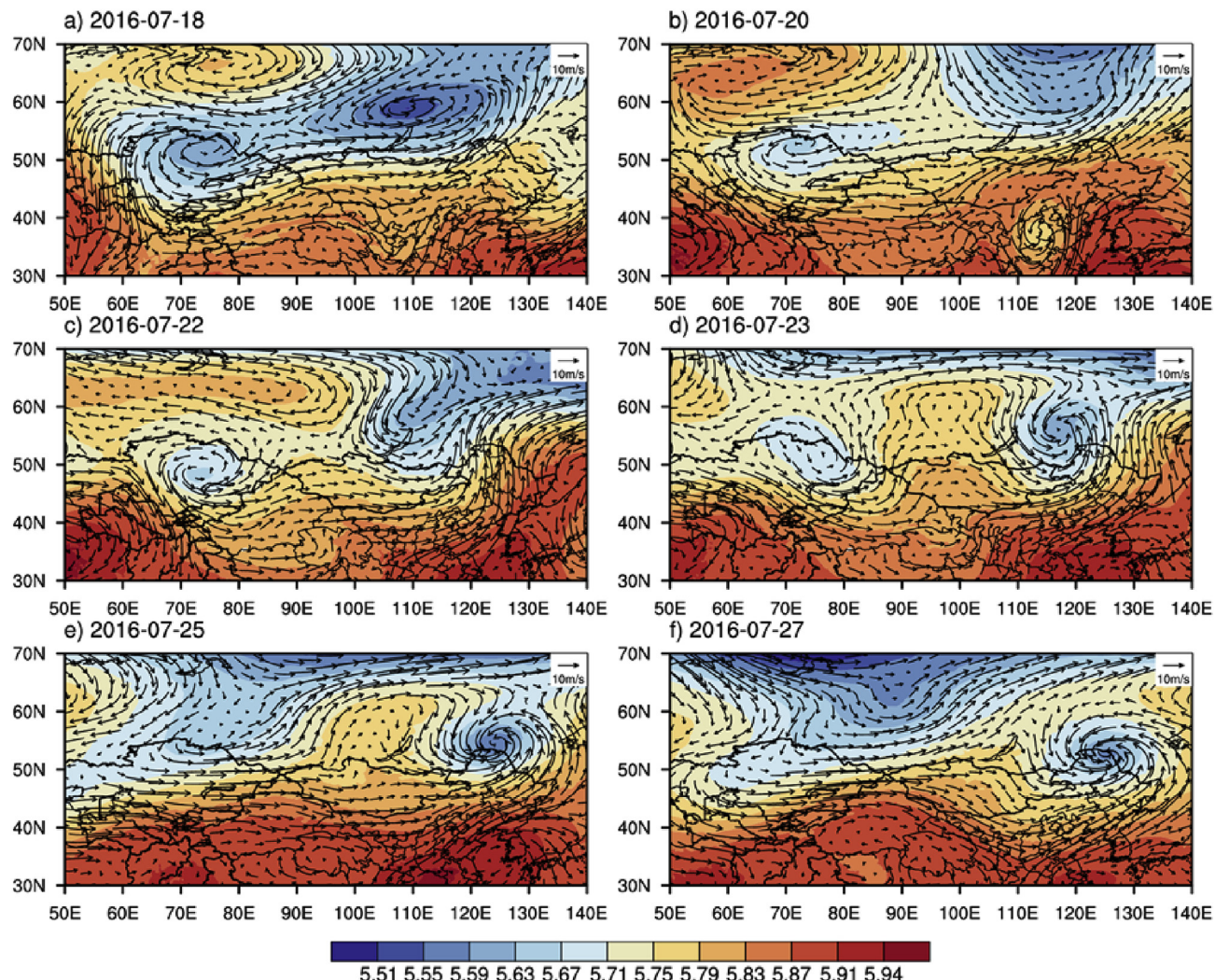


**Fig. 5.** Spatial distributions of the daily mean wind vector (arrows) and geopotential height (colors, blue for low and red for high) at 500 hPa from the WRF model (a–f) on 18 July, 20 July, 22 July, 23 July, 25 July and 27 July 2016.

### 3. Model description and setup

#### 3.1. WRF model

The WRF model (version 3.7.1) is used to simulate the weather processes. The WRF model also provides the initial field within the FLEXPART model during the smoke event; the model output is a 1-h interval, and the first 12 h are used for the spin-up. The 6-h National Centers for Environmental Prediction (NCEP) Final Analysis (FNL) dataset with a spatial resolution of  $1^\circ \times 1^\circ$  is used for the initial and boundary conditions. The center of the model domain is 50°N, 95°E. The horizontal grids are  $340 \times 165$  with a resolution of 30 km. Vertically, a total of 32 vertical levels are established from the surface to the altitude of 50 hPa. A WRF Single-Moment (WSM) 6-class graupel scheme is selected for the microphysics options, while the Rapid Radiation Transfer Model (RRTM) and the Dudhia scheme are used as the longwave and shortwave radiation schemes, respectively. Other details regarding the model options and WRF configurations in this study are listed in Table 1.

#### 3.2. FLEXPART-WRF model

The FLEXPART model, which is widely used to simulate mesoscale transport processes, the atmospheric water cycle, tropospheric-

stratospheric exchanges, and global pollutant transport as well as for many other aspects of research, describes the transport and diffusion processes of air parcels by calculating their trajectories (Stohl et al., 1998; Stohl and Thomson, 1999).

In this study, FLEXPART-WRF version 3.1, which is a version of FLEXPART that is executed using the WRF model output (Brioude et al., 2013), is used to simulate the transport and concentrations of smoke aerosols. The modeling domain encompasses 30–70°N and 50–140°E. The horizontal spatial and temporal resolutions are  $0.125^\circ \times 0.125^\circ$  and 1 h, respectively. A total of 8 vertical levels (50, 100, 500, 1000, 2000, 3000, 4000 and 5000 m) are established. The integral time of the numerical simulation spans from 00:00 UTC 17 July 2016 to 00:00 UTC 29 July 2016.

According to the time of the fire point appeared and disappeared, four aerosol sources were set up in FLEXPART-WRF model, including 81.5–94°E, 62.5–66.5°N (region A in Fig. 2), 92–106°E, 58–63°N (region B in Figs. 2), 74–79°E, 63.5–66.5°N (region C in Figs. 2) and 105.5–107.5°E, 54.5–56.5°N (region D in Fig. 2). The release time from these four sources are 17–23, 17–25, 19–24 and 12–28 July 2016, respectively. According to Damoah et al. (2004), we set  $10^5$  particles released from every source with 0–1.5 km release height in the model. Based on the flux data of BC from the CAMS Global Fire Assimilation System and vertical velocity data from the ERA5 dataset, the daily mean BC concentration within the smoke aerosol plumes was calculated

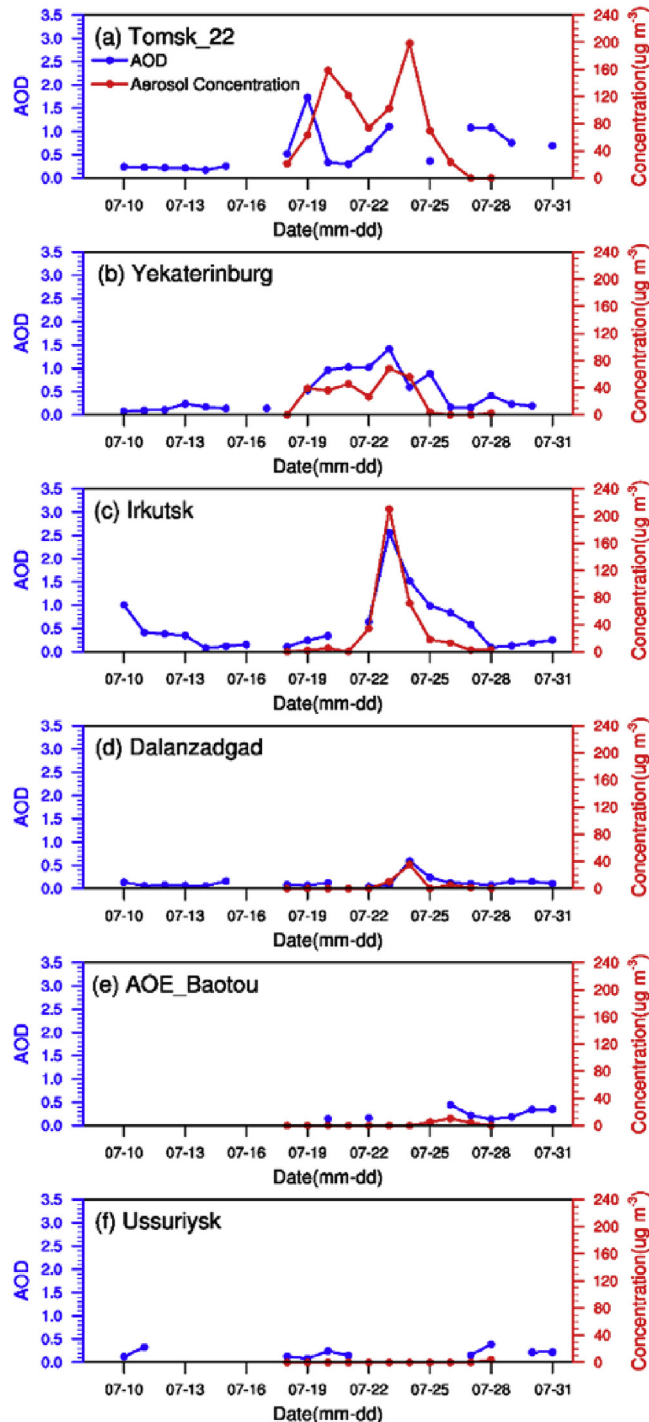


**Fig. 6.** Daily mean AERONET AOD at 500 nm (blue lines) and the daily mean aerosol concentration (red lines, units:  $\mu\text{g m}^{-3}$ ) at a height of 50 m simulated using the FLEXPART-WRF model at Tomsk\_22 (a), Yekaterinburg (b), Irkutsk (c), Dalanzadgad (d), AOE\_Baotou (e) and Ussuriysk (f) from 10 July to 31 July 2016. (For interpretation of the references to color in this figure legend, the reader is referred to the Web version of this article.)

over these four sources (According to formula (1)). The findings of Kozlov (2008) indicate that the BC concentration during the forest fire events that occurred in West Siberia from 1997 to 2005 was 1–4.5% of the total aerosol concentration, correspondingly, we assumed that the BC concentration during this forest fire event was 2.75% of the total aerosol concentration. Thus, the daily mean aerosol concentrations can be calculated. Basing on the daily mean aerosol concentration and the

volume of the release region, the aerosol mass was set up in FLEXPART-WRF model. Finally, basing on the estimate, the aerosol masses released from four aerosol sources in the FLEXPART model are set as  $2.5 \times 10^5 \text{ kg}$ ,  $8 \times 10^5 \text{ kg}$ ,  $1.2 \times 10^5 \text{ kg}$  and  $0.6 \times 10^5 \text{ kg}$ , respectively.

$$\text{Concentration} = \text{Flux} * \omega^{-1} \quad (1)$$

## 4. Results and discussion

### 4.1. Detection of the smoke event from Russian forest fires

The CALIPSO products, which can be used to observe aerosols over a bright surface and beneath thin clouds under clear-sky conditions (Vaughan et al., 2004; Winker et al., 2006), are used to identify smoke aerosols in this study. According to the results of Omar et al. (2009), the total attenuated backscatter coefficient at 532 nm of the aerosol particles is concentrated within the range from 0.003 to  $0.009 \text{ km}^{-1}\text{sr}^{-1}$ , and the threshold for extracting the aerosol top height is  $0.0015 \text{ km}^{-1}\text{sr}^{-1}$ . The depolarization ratio of aerosols originating from biomass burning is between 0.03 and 0.11 (Chiang et al., 2007; Huang et al., 2007; Xie et al., 2008).

An analysis based on the CALIPSO products reveals that a large quantity of aerosols was present over Siberia. Fig. 1 shows the altitude-orbit cross-section of the total attenuated backscattering intensity (a1-a2), depolarization ratio (b1-b2) and spatial distribution of cloud and aerosol types (c1-c2) on 18 July 2016. The satellite orbit paths are presented in Fig. 2; the blue and red lines denote the orbits scanned at 20:32 and 22:10, respectively. In panels a1-a2 of Fig. 1, the gray shading indicates the topography, the white parts are clouds, and the deep blue area denotes the region blocked by clouds that is without signal.

As shown in panels a1-a2 and b1-b2 of Fig. 1, the total attenuated backscatter coefficient and volume depolarization ratio are  $0.003\text{--}0.008 \text{ km}^{-1}\text{sr}^{-1}$  and 0–0.4, respectively. In particular, over the area between  $55^\circ\text{N}$  and  $70^\circ\text{N}$ , the total attenuated backscatter values are large and the volume depolarization ratio ranges from 0.06 to 0.2; these values indicate that the main component is represented by smoke aerosols over Siberia and that the smoke plumes could have extended upward to approximately 3 km. As shown in panels c1 and c2 of Fig. 1, smoke aerosols can be observed over Siberia on 18 July 2016, while dust, polluted dust and polluted continental dust are simultaneously detected.

To verify the existence of the smoke event on 18 July 2016 over the study area, the MODIS image acquired from Terra was examined. As shown in Fig. 2, the MODIS image reveals the presence of aerosol plumes over Siberia on 18 July 2016. According to the report provided by the Global Fire Monitoring Center (<http://www.fire.uni-freiburg.de/GFMnew>), a total of 6028 fires were detected on 20 July 2016 throughout Siberia ( $50\text{--}70^\circ\text{N}$ ;  $60\text{--}140^\circ\text{E}$ ), thereby affecting 5.19 million hectares of forested area and other lands.

Furthermore, thermal anomalies and fires from the MOD14 data were analyzed. During the period of 17–28 July 2016, an accumulation of 11708 hot spots were detected (Fig. 3) in the vast area from the Lake Baikal to the Gulf of Ob, where the vegetation coverage is high. This confirms that extensive forest fires occurred throughout Central Siberia, particularly in the Tungus Plateau. Therefore, smoke aerosols were produced by the forest fire event that occurred during the period of 17–28 July 2016.

### 4.2. Transport of smoke aerosols to Asia

To investigate the transport processes of smoke aerosols from the Russia forest fire event, the aerosol mass column loading was simulated using the FLEXPART-WRF model. As shown in Fig. 4, the spatial distribution of the simulated aerosol mass column loading is in good

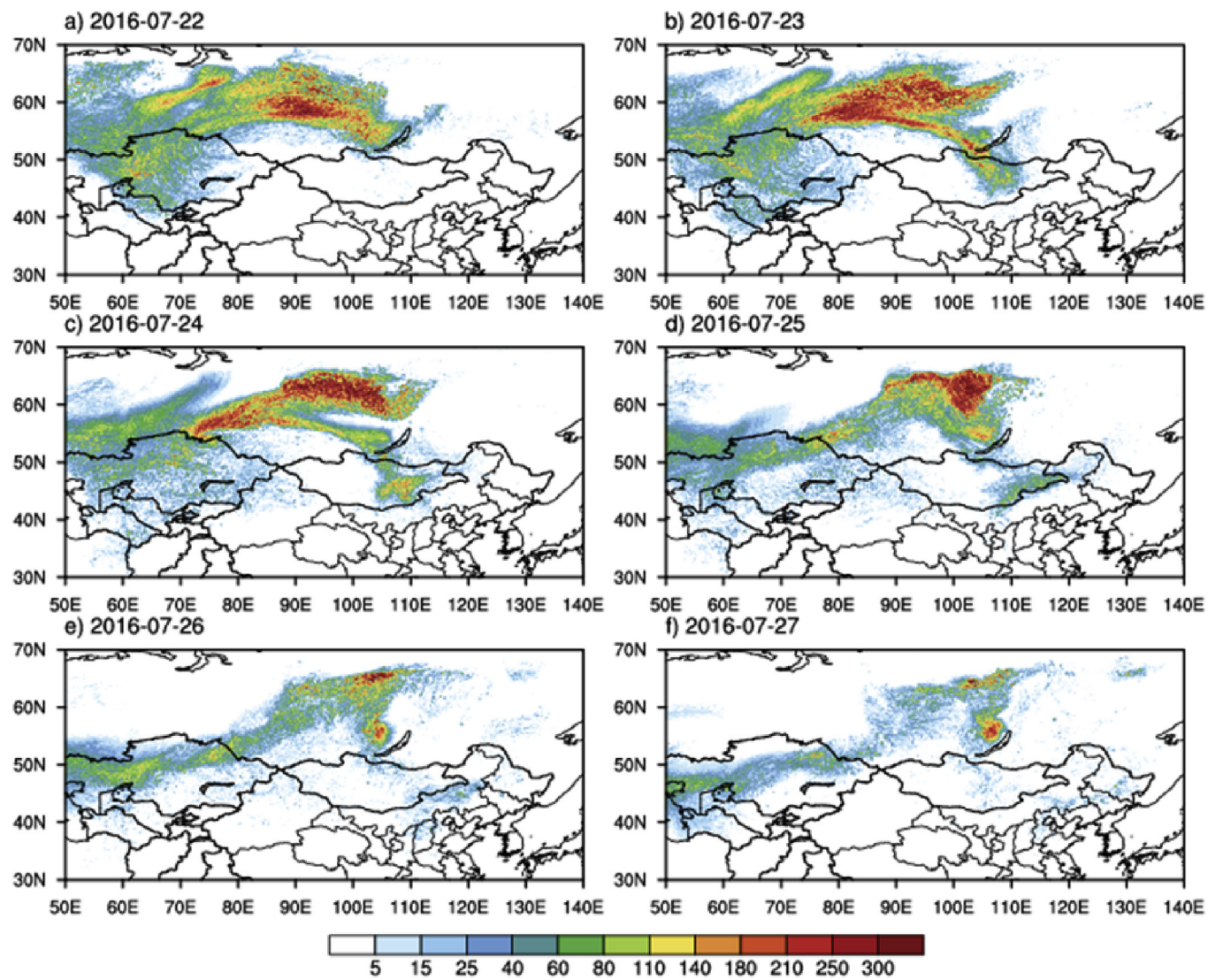


Fig. 7. Distribution of the aerosol concentration (units:  $\mu\text{g m}^{-3}$ ) simulated using the FLEXPART-WRF model at an altitude of 50 m from 22 July to 27 July 2016.

**Table 2**

FLEXPART-WRF simulated daily mean aerosol concentrations (units:  $\mu\text{g m}^{-3}$ ) in five cities during the Russia forest fire event of July 2016.

Cities	Date										
		7.19	7.20	7.21	7.22	7.23	7.24	7.25	7.26	7.27	7.28
Astana	0.00	23.13	13.56	72.44	29.22	123.06	54.89	42.80	20.48	5.18	
Tashkent	0.00	0.00	0.00	30.61	46.16	19.97	16.17	0.00	0.00	0.00	
Ulan Bator	0.00	0.00	0.00	5.43	92.03	77.09	42.67	30.41	15.39	3.98	
Altay	0.00	0.00	0.00	0.00	2.64	13.55	0.00	0.00	0.00	0.00	
Hulunbuir	0.00	0.00	0.00	0.00	0.00	0.00	58.91	39.14	0.00	0.00	

agreement with the MODIS-observed AODs over the study area. Overall, the FLEXPART-WRF model can effectively simulate the transport of smoke plumes. During the forest fire event, the AODs and mass column loadings exhibited high values over almost the entire Siberian region with values greater than 3.0 and  $400 \text{ mg m}^{-2}$ , respectively. Fig. 4 also demonstrates that smoke plumes originating from the forest fires over Central Siberia began to increase on 18 July 2016 (Fig. 4a1 and b1) and then moved westward to West Siberia with increasing AODs and concentrations over the following days (Fig. 4a2 and b2). On 23 July (Fig. 4c1 and c2), the smoke plumes had spread into the hinterlands of Central Asia, thereby affecting the air quality near the Aral Sea. Thereafter, weak smoke plumes were observed entering Xinjiang

Province of China on 25 July (Fig. 4d1 and d2). Meanwhile, with the westward transporting to Central Asia, it is especially interesting that the smoke plumes appeared to extend another branch across Lake Baikal on 23 July (Fig. 4c1 and c2) and then moved eastward and southward. As shown in Fig. 4c1 and c2, the smoke plumes emitted from the areas surrounding Lake Baikal began to move southward on 22 July (figure omitted) and arrived over Mongolia on 23 July. Subsequently, the smoke plumes gradually dispersed over the Inner Mongolia Autonomous Region on 25 July (Fig. 4d1 and d2) and over Northeast China on 27 July (Fig. 4e1 and e2). Meanwhile, the smoke plumes also moved eastward to the Russian Far East during the period of 25–27 July (Fig. 4d1–e2).

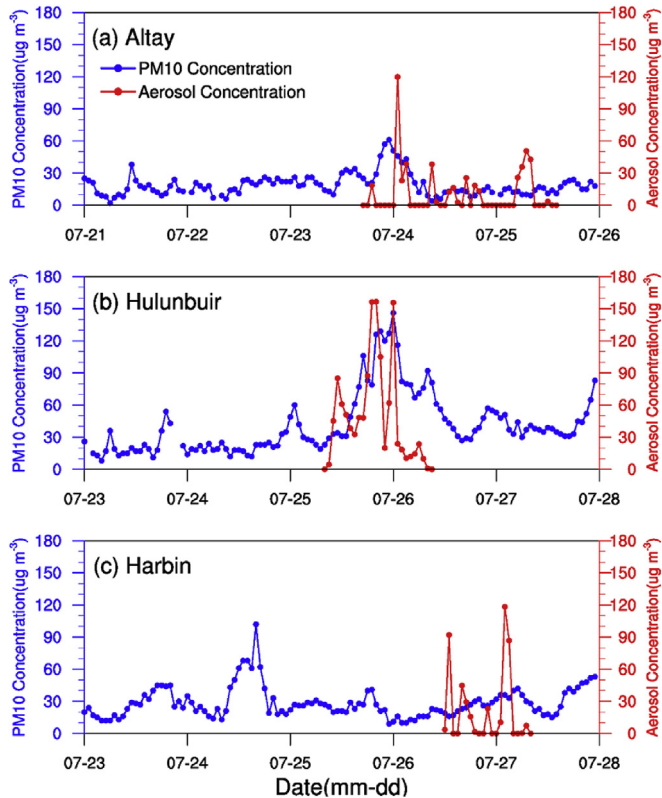


**Fig. 8.** Hourly real-time PM10 concentrations (blue lines, units:  $\mu\text{g m}^{-3}$ ) and hourly aerosol concentrations (red lines, units:  $\mu\text{g m}^{-3}$ ) at Altay (a), Hulunbuir (b) and Harbin (c) during the Russia forest fire event of July 2016. (For interpretation of the references to color in this figure legend, the reader is referred to the Web version of this article.)

As many studies have indicated (Bozier et al., 2007; Damoah et al., 2004; Dirksen et al., 2009; Miller et al., 2011; Sang et al., 2011), the transport of smoke plumes is principally driven by meteorological circulation. Fig. 5 displays the geopotential height and wind vector at 500 hPa derived from the WRF simulations during the period of this fire event. Two obvious cyclones can be found over Central Asia and Central Siberia (Fig. 5a). Influenced by these two cyclones, a strong easterly wind directed from Central Siberia to West Siberia drove the smoke plumes to move westward into Central Asia. The low-pressure weather system gradually separated and weakened on 20 July as it continued to move eastward (Fig. 5b). Thereafter, it gradually turned into a classic type of system with two troughs and one ridge (Fig. 5c and d). Subsequently, the low-pressure system located over Central Siberia moved southeastward and turned into the northeast vortex persisting over Northeast China (Fig. 5e–f), while the cyclone over Central Asia continued until 23 July. The eastward-moving low-pressure system located over Central Siberia caused strong northerly winds, thereby inducing the southward transport of smoke plumes across Mongolia into Northeast China, particularly on 23 July (Fig. 5d). Then, the cyclone over Central Asia was replaced by a new low-pressure system (Fig. 5e–f). Westerly winds that appeared in Kazakhstan as a result of this low-pressure system could have caused the smoke plumes over Central Asia to shift toward Xinjiang Province of China.

Fig. 6 shows the variations in the daily mean 500 nm AODs observed at the AERONET sites, which are denoted by blue triangles in Fig. 3, and the FLEXPART-WRF model aerosol concentrations at a height of 50 m. As indicated in Fig. 6, the FLEXPART-WRF model was capable of effectively simulating the transport of aerosols. Increased AODs and aerosol concentrations were observed at each site at different times based on the distance from the aerosol sources and on the transport pathways of the smoke plumes originating from the Russian forest fire

event. The AOD (500 nm) over Tomsk\_22 (Fig. 6a) situated along the westward transport path of the smoke aerosols discussed above jumped to 1.73 on 19 July, and the AOD peaked over Yekaterinburg with a value of 1.42 after 4 days due to westward transport (Fig. 6b), indicating that the smoke aerosols passed through Tomsk\_22 before reaching Yekaterinburg. The simulated aerosol concentrations peaked at  $198.87 \mu\text{g m}^{-3}$  and  $67.96 \mu\text{g m}^{-3}$  over the stations at Tomsk\_22 (Fig. 6a) and Yekaterinburg (Fig. 6b), respectively, in accordance with the AOD variations. Along the southeastward transport path, the AODs (500 nm) observed at the AERONET stations peaked successively on 23 July, 24 July, 25 July, 26 July, and 28 July at Irkutsk (Fig. 6c), Dalaanzadgad (Fig. 6d), AOE\_Baotou (Fig. 6e) and Ussuriysk (Fig. 6f), respectively. The FLEXPART-WRF model simulation revealed similar results. Overall, the AOD observations and model-simulated aerosol concentrations verify the existence of two transport paths.

#### 4.3. Quantification of the impact of transported smoke aerosols on Asia

Fig. 7 displays the distribution of the daily mean aerosol concentration at 50 m simulated using the FLEXPART-WRF model from 22 July to 27 July 2016. Due to the westward transport of the smoke aerosols, a large number of particles blanketed Central Asia with a high concentration of  $5\text{--}210 \mu\text{g m}^{-3}$  on 22 July (Fig. 7a). As a consequence of subsequent particle diffusion, the influenced area was expanded to Turkmenistan (Fig. 7b–d) coincident with a decrease in the particle concentration (Fig. 7b–f). On 24 July, as shown in Fig. 7c, the particles extended over the western border of Xinjiang Province of China with a concentration of  $5\text{--}80 \mu\text{g m}^{-3}$ . On 25 July, both the concentration and the coverage of particles over Central Asia began to decrease (Fig. 7d). Meanwhile, the southeastward transported particles with a concentration of  $40\text{--}250 \mu\text{g m}^{-3}$  entered central east area of Mongolia on 23 July (Fig. 7b) and then particles moving southward and eastward entered Hulunbuir on 26 July. Finally, relatively few aerosol particles entered Northeast China with a concentration of  $5\text{--}80 \mu\text{g m}^{-3}$  on 27 July. Table 2 summarizes the simulated aerosol concentrations in five cities (Astana, Tashkent, Ulan Bator, Altay and Hulunbuir) during the Russia forest fire event of July 2016. The smoke aerosols from Russian forest fires have the most lasting and intense impact on Central Asia, the impact on Mongolia is the next in importance, and the impact on China is the least intensity.

To explore the impact of the transported smoke aerosols on the air quality over Asia, ground-based measurements from three observation sites (denoted by the purple squares in Fig. 2) from the China Environmental Monitoring Network were analyzed. The observed hourly real-time PM10 and simulated aerosol concentrations at the Altay, Hulunbuir and Harbin stations during the event are shown in Fig. 8. The observed PM10 and FLEXPART-WRF-simulated aerosol concentrations at the three sites both increased initially and then decreased gradually after reaching their peak values in accordance with the transport processes discussed above (Figs. 3–6). These results imply that the smoke plumes originating from the Russia forest fires may have contributed to the increased PM10 concentration over Northern China. To confirm the contribution of the smoke aerosols to the Northern China PM10 concentration, the distributions of the optical depths of different aerosol types on 20 July 2016 derived from CAMS near-real-time data were analyzed (Fig. 9).

Comparing with Fig. 4b1, the spatial distribution of the total AOD over Russia derived from the CAMS data (Fig. 9a) is in good agreement with that derived from the MODIS data. The difference in the total AOD between these two datasets over the Taklimakan Desert is probably due to a defect in the MODIS sensor with regard to the detection of aerosols over bright surfaces. Therefore, in this study, the CAMS data are deemed reliable for studying the temporal and spatial distributions of different aerosol types. As shown in Fig. 9, dust, organic matter, and sulfate aerosols are the dominant aerosols over the study area and are consequently analyzed in detail hereafter.

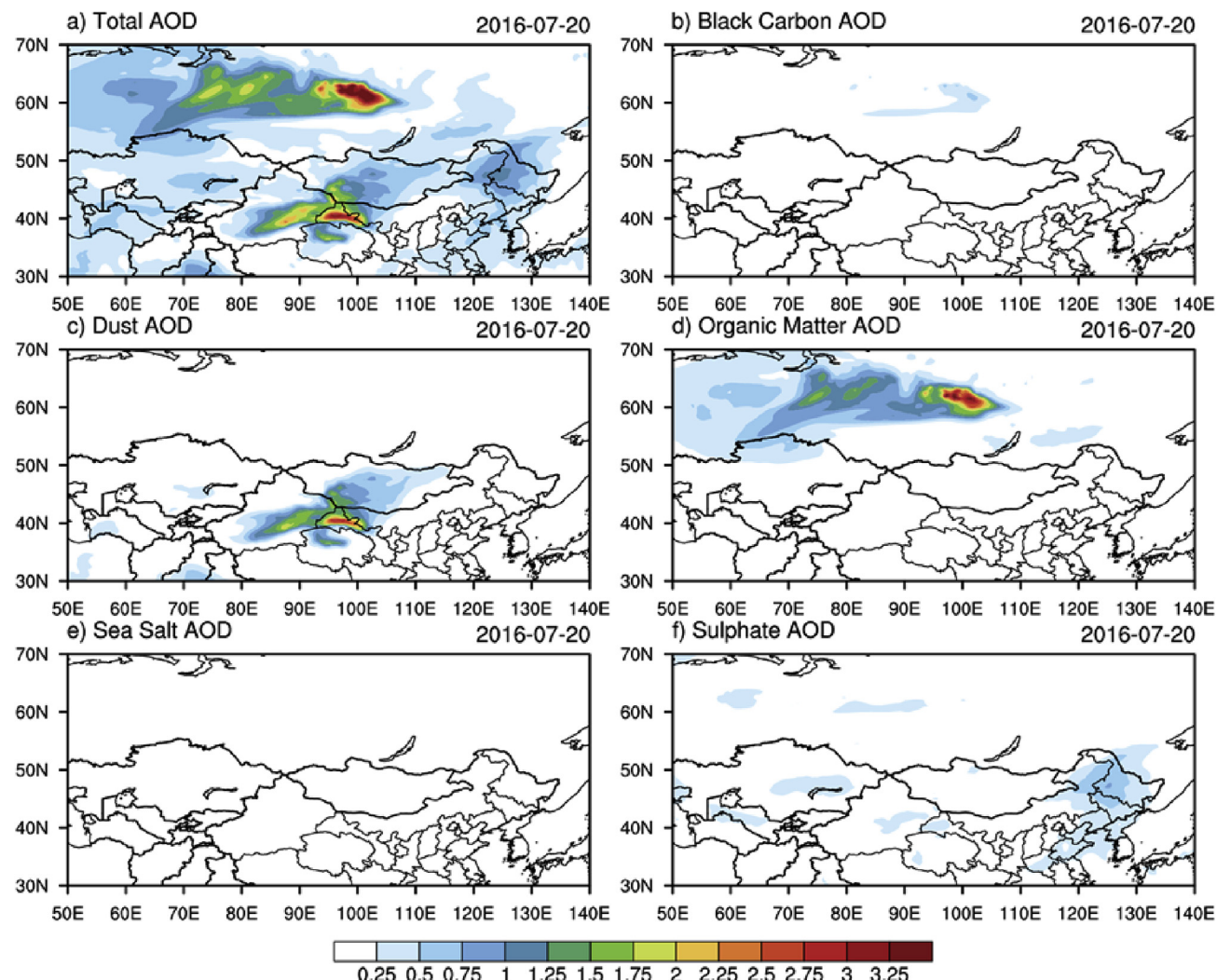


**Fig. 9.** Distribution of the total AOD (a), black carbon AOD (b), dust AOD (c), organic matter AOD (d), sea salt AOD (e) and sulfate AOD (f) from CAMS on 20 July 2016.

**Fig. 10** shows the distributions of the daily mean AODs of dust (a1 and d1), organic matter (a2 and d2) and sulfates (a3 and d3) derived from CAMS near-real-time data during the period of 24–27 July 2016. As shown in **Fig. 10** a2, a large organic matter AOD can be observed at Altay; this variation corresponds to the PM10 concentration change shown in **Fig. 8a**. The PM10 concentration detected at the Altay station began to increase at 10:00 LST and peaked with a value of  $61 \mu\text{g m}^{-3}$  at 23:00 LST on 23 July (**Fig. 8a**). This high PM10 concentration continued until 7:00 on 24 July at Altay, which corresponds to the high AOD of organic matter shown in **Fig. 10** a2. This implies that the PM10 variations around Altay were mainly caused by smoke aerosols transported from the Russian forest fires. The variations in the PM10 concentration at Hulunbuir were similar to those over Altay (**Fig. 8b**). **Fig. 10** b2 and c2 also reveal that the contributions from sulfate and dust aerosols to the air pollution over Northern China can almost be ignored compared with the contribution from organic matter aerosols. The impact of smoke aerosols from Russian forest fires on the air quality over Hulunbuir may have lasted for 23 h. As shown in **Fig. 8c**, a high PM10 concentration can also be observed at the Harbin station, although there is a distinct difference in the concentration compared with that at Hulunbuir. Due to contributions from the long-distance transport of dust (**Fig. 10** a1), the PM10 concentration at Harbin reached its first peak with a value of  $102 \mu\text{g m}^{-3}$  and then quickly declined. Thereafter, the PM10 concentration began to increase at 00:00 LST on

July 26 and peaked again with a value of  $42 \mu\text{g m}^{-3}$  at 05:00 LST on July 27. The variations in the PM10 concentration during the period of 26–27 July 2016 were mainly caused by organic matter aerosols produced by the Russian forest fires, as is shown in **Fig. 10** c2 and d2. Meanwhile, the distributions of the daily mean AODs of organic matter also shows that abundant smoke aerosols were produced during Russian forest fires and transport to Asia. **Table 3** summarizes the ground-based observed PM10 and PM2.5 measurements and the simulated aerosol concentrations using the FLEXPART-WRF model at these three stations. The averaged PM10 concentrations during the period of Russian forest fires in July 2016 were  $22.79 \mu\text{g m}^{-3}$ ,  $60.46 \mu\text{g m}^{-3}$ , and  $26.83 \mu\text{g m}^{-3}$  at Altay, Hulunbuir, and Harbin, respectively. And the averaged PM2.5 concentrations at these three stations were  $8.51 \mu\text{g m}^{-3}$ ,  $34.77 \mu\text{g m}^{-3}$ , and  $15.42 \mu\text{g m}^{-3}$ , respectively. These values can be compared with aerosol concentrations simulated using the FLEXPART-WRF model during this period.

## 5. Conclusions

In this study, the transport of smoke aerosols originating from Russian forest fires that occurred during the period of 17–28 July 2016 was investigated using the FLEXPART-WRF model combined with aerosol observations and reanalysis data. Simultaneously, the impacts of this forest fire event on the air quality over Asia were also analyzed.

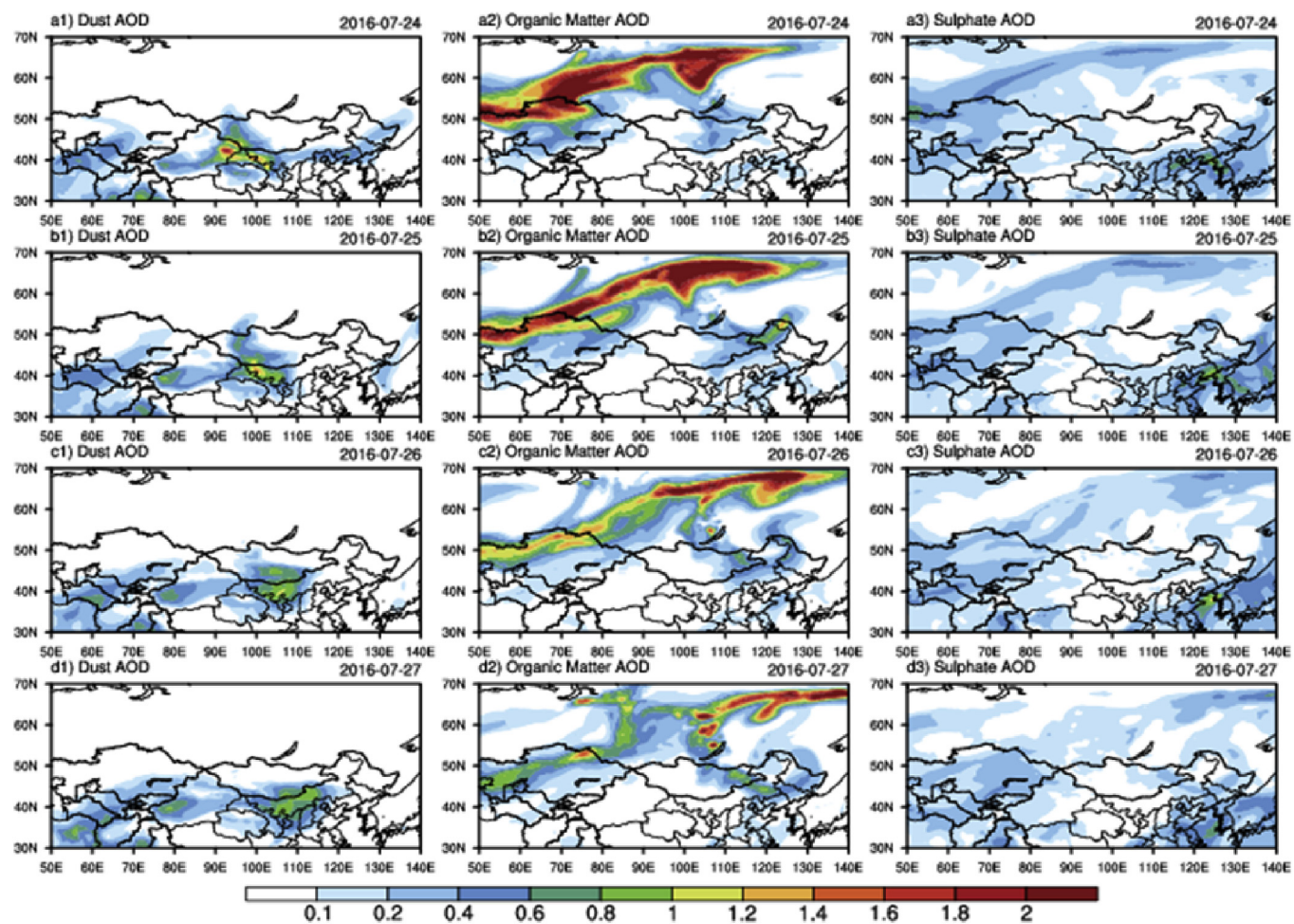


**Fig. 10.** Daily mean distribution of the dust AOD (a1-d1), organic matter AOD (a2-d2) and sulfate AOD (a3-d3) from CAMS data from 24 July to 27 July 2016.

**Table 3**

Statistical analysis of the observed hourly PM10 and PM2.5 and simulated aerosol concentrations during the Russia forest fire event of July 2016.

Stations	PM10 Concentration ( $\mu\text{g m}^{-3}$ )			PM2.5 Concentration ( $\mu\text{g m}^{-3}$ )			Simulated Aerosol Concentration ( $\mu\text{g m}^{-3}$ )		
	Mean	Max.	Min.	Mean	Max.	Min.	Mean	Max.	Min.
<b>Altay</b>									
23-07-2016	27.04	61	10	9.63	15	5	2.64	18.52	0
24-07-201	18.54	51	4	7.38	33	3	13.55	119.80	2.74
Averaged	22.79	56	7	8.51	24	4	8.10	138.32	1.37
<b>Hulunbuir</b>									
25-07-2016	59.03	129	19	31.96	85	3	58.91	156.55	4.49
26-07-2016	61.88	146	27	37.58	87	14	39.14	155.69	10
Averaged	60.46	137.5	23	34.77	86	8.5	49.03	156.12	7.25
<b>Harbin</b>									
26-07-2016	19.83	32	10	11.21	15	8	17.53	92.07	1.6
27-07-2016	33.83	53	15	19.63	34	13	31.88	118.33	0.33
Averaged	26.83	42.5	12.5	15.42	24.5	10.5	24.71	105.2	0.97

Smoke aerosols were observed during heavy forest fires that occurred throughout Russia using CALIPSO satellite products. The MODIS-observed AODs are greater than 3. Driven by meteorological conditions, the smoke aerosols were transported from Siberia to Xinjiang Province and Northeast China after passing through Mongolia and Central Asia. Combining the FLEXPART-WRF simulations with ground-based measurements, the FLEXPART-WRF simulations are deemed capable of accurately simulating the long-distance transport of aerosols. From these simulations, the smoke aerosols from Russian forest fires can influence Central Asia, Mongolia and China, in which the impacts on Central Asia and Mongolia last for nine and seven days,

respectively. Meanwhile, the smoke plumes from Russia evidently affected the air quality over Northern China with a peak PM10 concentration reaching  $146 \mu\text{g m}^{-3}$ . Although numerous studies have proven that dust and haze events have a substantial impact on the air quality over Asia, the contributions from smoke aerosols originating from Russian heavy forest fires should not be ignored.

#### Acknowledgments

This research was mainly supported by the National Natural Science Foundation of China (91744311). It was also jointly supported by the

National Natural Science Foundation of China (91737101 and 41475095), the Fundamental Research Funds for the Central Universities (Izujbky-2017-63), and the China 111 project (B13045).

## References

- Albrecht, B.A., 1989. Aerosols, cloud microphysics, and fractional cloudiness. *Science* 245 (4923), 1227–1230. <http://dx.doi.org/10.1126/science.245.4923.1227>.
- Bozier, K.E., Pearson, G.N., Collier, C.G., 2007. Doppler lidar observations of Russian forest fire plumes over Helsinki. *Weather* 62 (8), 203–208. <http://dx.doi.org/10.1002/wea.48>.
- Brioude, J., Cooper, O.R., Feingold, G., Trainer, M., Freitas, S.R., Kowal, D., Ayers, J.K., Prins, E., Minnis, P., McKeen, S.A., Frost, G.J., Hsie, E.-Y., 2009. Effect of biomass burning on marine stratocumulus clouds off the California coast. *Atmos. Chem. Phys.* 9, 8841e8856.
- Brioude, J., Arnold, D., Stohl, A., Cassiani, M., Morton, D., Seibert, P., Angevine, W., Evan, S., Dingwell, A., Fast, J.D., Easter, R.C., Pisso, I., Burkhardt, J., Wotawa, G., 2013. The Lagrangian particle dispersion model flexpart-wrf version 3.0. *Geosci. Model Dev.* 6 (6), 1889–1904. <http://dx.doi.org/10.5194/gmd-6-1889-2013>.
- Chiang, C.W., Chen, W.N., Liang, W.A., Das, S.K., Nee, J.B., 2007. Optical properties of tropospheric aerosols based on measurements of lidar, sun-photometer, and visibility at Chung-Li (25°N, 121°E). *Atmos. Environ.* 41 (19), 4128–4137. <http://dx.doi.org/10.1016/j.atmosenv.2007.01.019>.
- Christopher, S.A., Kliche, D.V., Chou, J., Welch, R.M., 1996. First estimates of the radiative forcing of aerosols generated from biomass burning using satellite data. *J. Geophys. Res. Atmos.* 101 (D16), 21265–21273. <http://dx.doi.org/10.1029/96JD02161>.
- Chubarova, N., Nezval, Y., Sviridenkov, M., Smirnov, A., 2012. Smoke aerosol and its radiative effects during extreme fire event over central Russia in summer 2010. *Atmos. Meas. Tech* 5 (3), 557–568. <http://dx.doi.org/10.5194/amtd-4-6351-2011>.
- Conard, S.G., Ivanova, G.A., 1997. Wildfire in Russian boreal forests: potential impacts of fire regime characteristics on emissions and global carbon balance estimates. *Environ. Pollut.* 98 (3), 305–313. [http://dx.doi.org/10.1016/S0269-7491\(97\)00140-1](http://dx.doi.org/10.1016/S0269-7491(97)00140-1).
- Crutzen, P.J., Andreae, M.O., 1990. Biomass burning in the tropics: impact on atmospheric chemistry and biogeochemical cycles. *Science* 250 (4988), 1669–1678. <http://dx.doi.org/10.1126/science.250.4988.1669>.
- Damoah, R., Spichtinger, N., Forster, C., James, P., 2004. Around the world in 17 days – hemispheric-scale transport of forest fire smoke from Russia in May 2003. *Atmos. Chem. Phys.* 4 (5), 1449–1471. <http://dx.doi.org/10.5194/acp-4-1311-2004>.
- Dirksen, R.J., Boersma, F.K., Laat, D.J., Stammes, P., Van, d.W.G.R., Val Martin, M., Kelder, H.M., 2009. An aerosol boomerang: rapid around-the-world transport of smoke from the December 2006 Australian forest fires observed from space. *J. Geophys. Res. Atmos.* 114 (D21). <http://dx.doi.org/10.1029/2009JD012360>.
- Dreessen, J., Sullivan, J., Delgado, R., 2016. Observations and impacts of transported Canadian wildfire smoke on ozone and aerosol air quality in the Maryland region on June 9–12, 2015. *J. Air Waste. Manage.* 66 (9), 842–862. <http://dx.doi.org/10.1080/10962247.2016.1161674>.
- Forster, C., Wandinger, U., Wotawa, G., James, P., Mattis, I., Althausen, D., Simmonet, P., O'Doherty, S., Jennin, S.G., Kleefel, C., Schneid, J., Trick, T., Kreip, S., Jager, H., Stohl, A., 2001. Transport of boreal forest fire emissions from Canada to Europe. *J. Geophys. Res. Atmos.* 106 (D19), 22887–22906. <http://dx.doi.org/10.1029/2001JD900115>.
- Gorchakova, I.A., Mokhov, I.I., 2012. The radiative and thermal effects of smoke aerosol over the region of Moscow during the summer fires of 2010. *Izv. Atmos. Ocean. Phys.* 48 (5), 496–503. <http://dx.doi.org/10.1134/S0001433812050039>.
- Han, Z., Li, J., Guo, W., Xiong, Z., Zhang, W., 2013. A study of smoke radiative feedback on smoke cycle and meteorology over East Asia by a coupled regional climate-aerosol model. *Atmos. Environ.* 68 (1), 54–63. <http://dx.doi.org/10.1016/j.atmosenv.2012.11.032>.
- Haywood, J., Boucher, O., 2000. Estimates of the direct and indirect radiative forcing due to tropospheric aerosols: a review. *Rev. Geophys.* 38 (4), 513–543. <http://dx.doi.org/10.1029/1999RG000078>.
- Hersbach, H., 2016. The ERA5 Atmospheric Reanalysis. AGU Fall Meeting. AGU Fall Meeting Abstracts.
- Huang, J., Minnis, P., Yi, Y., Tang, Q., Wang, X., Hu, Y., Liu, Z., Ayers, K., Trepte, C., Winker, D., 2007. Summer dust aerosols detected from CALIPSO over the Tibetan plateau. *Geophys. Res. Lett.* 34 (18), 529–538. <http://dx.doi.org/10.1029/2007GL029938>.
- Huang, J., Wang, T., Wang, W., Li, Z., Yan, H., 2014. Climate effects of dust aerosols over East Asian arid and semiarid regions. *J. Geophys. Res. Atmos.* 119 (19), 11,398–11,416. <http://dx.doi.org/10.1002/2014JD021796>.
- Jia, R., Liu, Y., Chen, B., Zhang, Z., Huang, J., 2015. Source and transportation of summer dust over the Tibetan Plateau. *Atmos. Environ.* 123, 210–219. <http://dx.doi.org/10.1016/j.atmosenv.2015.10.038>.
- Kahn, R.A., Li, W., Moroney, C., Diner, D.J., Martonchik, J.V., Fishbein, E., 2007. Aerosol source plume physical characteristics from space-based multiangle imaging. *J. Geophys. Res.* 112 (D11). <http://dx.doi.org/10.1029/2006JD007647>.
- Kahn, R.A., Chen, Y., Nelson, D.L., Leung, F., Li, Q., Diner, D.J., Logan, J.A., 2008. Wildfire smoke injection heights: two perspectives from space. *Geophys. Res. Lett.* 35 (4), 228–236. <http://dx.doi.org/10.1029/2007GL032165>.
- Koren, I., Martins, J.V., 2004. Measurement of the effect of Amazon smoke on inhibition of cloud formation. *Science* 303 (5662), 1342–1345. <http://dx.doi.org/10.1126/science.1089424>.
- Kozlov, V.S., 2008. Mass fraction of black carbon in submicron aerosol as an indicator of influence of smoke from remote forest fires in Siberia. *Atmos. Environ.* 42 (11), 2611–2620. <http://dx.doi.org/10.1016/j.atmosenv.2007.07.036>.
- Kozlov, V.S., Panchenko, M.V., Pol'kin, V.V., Pkhalagov, Y.A., Uzhegov, V.N., Shchelkanov, N.N., Yasheva, E.P., 1999. Some peculiarities in the dynamics of optical and microphysical characteristics of aerosol in smoke haze. *J. Aerosol Sci.* 12 (5), 390–394.
- Lee, K.H., Kim, J.E., Kim, Y.J., Kim, J., Hoyningen-Huene, W.V., 2005. Impact of the smoke aerosols from Russian forest fires on the atmospheric environment over Korea during May 2003. *Atmos. Environ.* 39 (1), 85–99. <http://dx.doi.org/10.1016/j.atmosenv.2004.09.032>.
- Liu, Y., Shi, G., Xie, Y., 2013. Impact of smoke aerosol on glacial-interglacial climate. *Adv. Atmos. Sci.* 30 (6), 1725–1731. <http://dx.doi.org/10.1007/s00376-013-2289-7>.
- Liu, Y., Jia, R., Dai, T., Xie, Y., Shi, G., 2014. A review of aerosol optical properties and radiative effects. *J. Meteor. Res.* 28 (6), 1003–1028. <http://dx.doi.org/10.1007/s13351-014-4045-z>.
- Liu, Y., Sato, Y., Jia, R., Xie, Y., Huang, J., Nakajima, T., 2015. Modeling study on the transport of summer dust and anthropogenic aerosols over the Tibetan Plateau. *Atmos. Chem. Phys.* 15 (21), 12581–12594. <http://dx.doi.org/10.5194/acp-15-15005-2015>.
- Martin, M.V., Logan, J.A., Kahn, R.A., Leung, F.Y., Nelson, D.L., Diner, D.J., 2009. Smoke injection heights from fires in north America: analysis of 5 years of satellite observations. *Atmos. Chem. Phys.* 9 (5), 20515–20566. <http://dx.doi.org/10.5194/acp-10-1491-2010>.
- Miller, D.J., Sun, K., Zondlo, M.A., Kanter, D., Dubovik, O., Welton, E.J., Winker, D.M., Ginoux, P., 2011. Assessing boreal forest fire smoke aerosol impacts on U.S. air quality: a case study using multiple data sets. *J. Geophys. Res. Atmos.* 116 (D22). <http://dx.doi.org/10.1029/2011JD016170>.
- Müller, D., Mattis, I., Wandinger, U., Ansmann, A., Althausen, D., Stohl, A., 2005. Raman lidar observations of aged Siberian and Canadian forest fire smoke in the free troposphere over Germany in 2003: microphysical particle characterization. *J. Geophys. Res. Atmos.* 110 (D17). <http://dx.doi.org/10.1029/2004JD005756>.
- Noh, Y.M., Müller, D., Dong, H.S., Lee, H., Jin, S.J., Lee, K.H., Cribbc, M., Li, Z.Q., Kim, Y.J., 2009. Optical and microphysical properties of severe haze and smoke aerosol measured by integrated remote sensing techniques in Gwangju, Korea. *Atmos. Environ.* 43 (4), 879–888. <http://dx.doi.org/10.1016/j.atmosenv.2008.10.058>.
- Nopmongcol, U., Khamwichit, W., Fraser, M.P., Allen, D.T., 2007. Estimates of heterogeneous formation of secondary organic aerosol during a wood smoke episode in Houston. *Texas. Atmos. Environ.* 41 (14), 3057–3070. <http://dx.doi.org/10.1016/j.atmosenv.2006.11.050>.
- Omar, A.H., Winker, D.M., Kittaka, C., Vaughan, M.A., Liu, Z., Hu, Y., Trepte, C.R., Rogers, R.R., Ferrare, R.A., Lee, K.-P., Kuehn, R.E., Hostettler, C.A., 2009. The Calipso automated aerosol classification and lidar ratio selection algorithm. *J. Atmos. Ocean. Technol.* 26 (10), 1994–2014. <http://dx.doi.org/10.1175/2009JTECHA1231.1>.
- Penner, J.E., Dickinson, R.E., O'Neill, C.A., 1992. Effects of aerosols from biomass burning on the global radiation budget. *Science* 256 (5062), 1432–1434. <http://dx.doi.org/10.1126/science.256.5062.1432>.
- Penner, J.E., Zhang, S.Y., Chuang, C.C., 2003. Soot and smoke aerosol may not warm climate. *J. Geophys. Res. Atmos.* 108 (D21). <http://dx.doi.org/10.1029/2003JD003409>.
- Rosário, N.E., Longo, K.M., Freitas, S.R., Yamasoe, M.A., Fonseca, R.M., 2013. Modeling the south American regional smoke plume: aerosol optical depth variability and surface shortwave flux perturbation. *Atmos. Chem. Phys.* 13 (6), 2923–2938. <http://dx.doi.org/10.5194/acp-13-2923-2013>.
- Sang, X.F., Chan, C.Y., Engling, G., Chan, L.Y., Wang, X.M., Zhang, Y.N., Shi, S., Zhang, Z.S., Zhang, T., Hu, M., 2011. Levoglucosan enhancement in ambient aerosol during springtime transport events of biomass burning smoke to southeast China. *Tellus B* 63 (1), 129–139. <http://dx.doi.org/10.1111/j.1600-0889.2010.00515.x>.
- Shukurov, K.A., Mokhov, I.I., Shukurova, L.M., 2014. Estimate for radiative forcing of smoke aerosols from 2010 summer fires based on measurements in the Moscow region. *Izv. Atmos. Ocean. Phys.* 50 (3), 256–265. <http://dx.doi.org/10.1134/S0001433814020091>.
- Sitnov, S.A., Gorchakov, G.I., Sviridenkov, M.A., Kopeikin, V.M., Ponomareva, T.Y., Karpov, A.V., 2013. The effect of atmospheric circulation on the evolution and radiative forcing of smoke aerosol over European Russia during the summer of 2010. *Izv. Atmos. Ocean. Phys.* 49 (9), 1006–1018. <http://dx.doi.org/10.1134/S0001433813090144>.
- Solomos, S., Amirdis, V., Zanis, P., Gerasopoulos, E., Sofiou, F.I., Herekakis, T., Brioude, J., Stohl, A., Kahn, R.A., Kontos, C., 2015. Smoke dispersion modeling over complex terrain using high resolution meteorological data and satellite observations - the FireHub platform. *Atmos. Environ.* 119, 348–361. <http://dx.doi.org/10.1016/j.atmosenv.2015.08.066>.
- Stocks, B.J., Goldammer, J.G., Cahoon, D.R., Cofer, W.R., 1998. Fire research in the boreal zone of Eurasia and North America. *IGAC Newsletter* 15, 13–15.
- Stohl, A., Thomson, D.J., 1999. A density correction for Lagrangian particle dispersion models. *Bound. -Lay. Meteorol* 90 (1), 155–167. <http://dx.doi.org/10.1023/A:1001741110696>.
- Stohl, A., Hittenberger, M., Wotawa, G., 1998. Validation of the Lagrangian particle dispersion model FLEXPART against large scale tracer experiment data. *Atmos. Environ.* 32 (24), 4245–4264. [http://dx.doi.org/10.1016/S1352-2310\(98\)00184-8](http://dx.doi.org/10.1016/S1352-2310(98)00184-8).
- Vaughan, M.A., Young, S.A., Winker, D.M., Powell, K.A., Omar, A.H., Liu, Z., Hu, Y., Hostettler, C.A., 2004. Fully automated analysis of space-based lidar data: an overview of the CALIPSO retrieval algorithms and data products. *Laser Radar Tech. Atmos. Sens* 5575, 16–30. <http://dx.doi.org/10.1117/12.572024>.
- Vinogradova, A.A., Smirnov, N.S., Korotkov, V.N., Romanovskaya, A.A., 2015. Forest fires in Siberia and the far east: emissions and atmospheric transport of black carbon to the

- arctic. *Atmos. Oceanic Opt* 28 (6), 566–574. <http://dx.doi.org/10.1134/S1024856015060184>.
- Winker, D., Vaughan, M., Hunt, B., 2006. The CALIPSO mission and initial results from CALIOP. *Proc. SPIE* 7. <http://dx.doi.org/10.1117/12.698003>.
- Xie, C., Nishizawa, T., Sugimoto, N., Matsui, I., Wang, Z., 2008. Characteristics of aerosol optical properties in pollution and Asian dust episodes over Beijing, China. *Appl. Optic.* 47 (27), 4945–4951. <http://dx.doi.org/10.1364/AO.47.004945>.
- Zhang, Z.S., Engling, G., Lin, C.Y., Chou, C.C.K., Lung, S.C.C., Chang, S.Y., Fan, S.J., Chan, C.Y., Zhang, Y.H., 2010. Chemical speciation, transport and contribution of biomass burning smoke to ambient aerosol in Guangzhou, a mega city of China. *Atmos. Environ.* 44 (26), 3187–3195. <http://dx.doi.org/10.1016/j.atmosenv.2010.05.024>.